**Model of T-cell nuclear deformation by the cortical actin layer**

**Running Title:** Actin mediated nuclear deformation

Gur Fabrikant[1,3], Soumya Gupta[2,3], GV Shivashankar[2]*, and Michael M Kozlov[1]*

[1]Department of Physiology and Pharmacology, Sackler Faculty of Medicine, Tel Aviv University, Ramat Aviv, 69978 Tel Aviv, Israel

[2]Mechanobiology Institute & Department of Biological Sciences, National University of Singapore, Singapore

[3]these authors contributed equally to this work

* Correspondence: shiva.gvs@gmail.com, michk@post.tau.ac.il

## Supplementary information

### Method of computations

*Equilibrium shapes and elastic moduli*

To describe the mutual deformation of the actin layer and the elastic shell representing the nucleus, we use the modified (compressible) Neo-Hookean model for isotropic materials (see derivation in [1],[2]).

The strain energy functional is given by:

$$\psi = \frac{1}{2}\mu\left(I_1 - 3\right) - \mu \ln J + \frac{1}{2}\lambda\left(\ln J\right)^2 \qquad \textbf{(1)}$$

where $\mu, \lambda$ are the Lame' coefficients which can be expressed through Young and Poisson moduli according to: $\mu = E/2\left(1+\nu\right)$ and $\lambda = E\nu/(2\left(1-2\nu\right)\left(1+\nu\right))$.

The isochoric and dilatational deformations are functions of the principal invariants of the right Cauchy strain tensor, $C$ [3,4], which are $I_1 = Tr\left(C\right)$ and $J = \det(F_{vol})$.

The equilibrium system configurations correspond to the minimum of the total elastic energy obtained by integration of (1) over the volume. The energy minimization was performed based on the weak form or virtual displacement principle according to standard Finite Element methods. To match the computed shapes of the nucleus shell and the actin layer (see below), we used the Lagrange-quadratic shape functions on

top of a triangular mesh which was manually refined towards the contact region between the two sub-systems. The assembly and solution were carried out by an Augmented Newton solver - available within the commercial software Comsol Multiphysics.

The first step and the main idea, was to make an educated guess of the possible shapes of the contact region between the two elastic bodies based on their initial unstressed shapes and (axial) symmetry. The simplest deformation contours for spherical compressions are elliptical arcs, thus a family of ellipsoids was used to approximate the equilibrium contour at the contact region. Second, we segregated the system into two complementary sub-systems (see Fig. S5): one representing the nucleus shell and the second modeling the cylindrical actin layer. The nucleus shell was compressed by an infinitely rigid concave scaffold to a final prolate ellipsoid with a pre-defined final equator radius. The actin layer was expanded by an infinitely rigid ellipsoid whose equator radius, *a*, equals that of the scaffold (see Fig. S5). In order to determine the tuning range for the ellipsoid polar radius, we noted that any isotropic shell under radial compression experiences a reduction of its area. For each value of the equator radius, *a*, we used an initial polar radius, *c*, that preserves the original nucleus area, $A_{tot}$, according to:

$$A_{tot} = 2\pi a^2 \left( 1 + \frac{\cos^{-1}(a/c)}{(a/c)\sqrt{1-(a/c)^2}} \right) \quad \textbf{(2)}$$

We then changed the shape of the ellipsoid by reducing *c* until the shapes of the deformed nucleus shell and actin layer coincided in all contact points. The resulting configuration represented a "contact ellipsoid" which was still not the correct solution for the whole system. Among all "contact ellipsoids", only the configuration that corresponded to a global minimum of the strain energy could be regarded as a physical solution. Thus in order to find the correct solutions, we recorded the "contact ellipsoid" dimensions, integrated over the elastic strain energies separately in both sub-systems and summed up the results into a total strain energy value $E_{tot} = \iiint_{nucleus} W_s dv + \iiint_{tube} W_s dv$.

By repeating this procedure with different elastic moduli for different values of the equator radii, we created the energy curves seen in Fig. S6. Note that the energy was calculated with respect to a global non-stressed state represented by the nucleus radius

equal to $2.8\mu m$ and the inner radius of the actin cylinder equal to $1\mu m$. The minimum of each curve in Fig. S6 represents a global minimum of the system energy, hence defining the equilibrium shape of the nucleus and tube for a given choice of elastic moduli- $E,\nu$.

*Estimation of the maximal forces and filament density at the cylindrical base of the polymerizing actin gel*

The maximum axial reaction force, needed for engulfing the nucleus, occurs when the nucleus is covered to its midst by the actin tube. Due to convergence problems of the used computer program, we were unable to compute directly the exact equilibrium shapes for partial engulfing. Therefore, we used the equilibrium shapes received for complete engulfing as an approximation for the shapes corresponding to half engulfing and used them for calculating the reaction forces that act from the bead to the base of the actin tube, which represent the force developed by actin polymerization.

Essentially, all elasticity-based contact problems admit two possible ways of calculating the overall reaction forces on some fixed boundary, direct and indirect ones. In the direct approach, the reaction (or polymerization) force on the bead can be calculated directly by integrating the axial stress component of the actin tube at the "fixed" cylindrical base ($z=12$): $f_z = \iint\limits_{A-bead} \sigma_{zz} dA$ (blue line Fig S7B). This force varies greatly as the nucleus penetrates and deforms the tube. It reaches a maximal value when the nucleus only "pushes in" on the tube– i.e. engulfed till its midst ( Fig S7B, blue curve at $\sim Z_{nuc} = 1\mu m$) and reaches ~ zero when the nucleus is fully covered by the tube. In this state, the nucleus "pushes in and out", symmetrically on the tube and the contributions to the overall force in the $\hat{z}$ direction cancel out each other (Fig S7B, blue curve at the lower right corner: $Z_{nuc} = 6\mu m$). Each of the blue triangles, mark a convergent solution which is later used for interpolating the maximal direct force at mid-penetration.

As the elastic moduli of the nucleus increase, thus leading to wider equatorial ellipsoids, the amount of converging points decreases till we are no longer able to properly interpolate the correct location and magnitude of the mid-penetration force.

For these cases, namely stiff nuclei with equilibrium equator radii $a_{eq} > 2\mu m$, we revert to the indirect estimation.

The indirect method suggested for this contact problem, involves the contact pressure profile of the deforming boundary and utilizes the symmetry of the final engulfed state (Fig S7B - red curve). We suggest that the contact pressure over half a nucleus in the final state is roughly the same as the contact pressure felt by the tube in mid-penetration. We therefore calculate the axial reaction force by integrating the $\hat{z}$-projection of the contact pressure profile over half a nucleus in the fully engulfed state: $f_z \approx \iint_{half\ nuc} T^{(n)} \cdot n_z da$. We were able to make sure that the indirect method gives an excellent approximation for the case of nuclei much softer than the actin layer as seen in Fig S7B (the value of the red curve at $z = 6$ approximately coincides with the maximal direct force - blue curve at $z = 1$ in Fig S7B.)

A careful inspection of these contact profiles as seen in Fig S7A, indeed confirms that half of the symmetrical profile at full engulfment ($z_{nuc} = 6\mu m$) is similar in shape and magnitude to the entire profile at mid-penetration ($z_{nuc} \sim 1\mu m$). Moreover, we should emphasize that the only "true" profile among these profiles (Fig S7A) is the fully engulfed configuration ($z_{nuc} = 6\mu m$). "True" in the sense that it corresponds to a state of a total minimal energy and is identical in both parts of the segregated system as required by force balance principle. The other profiles stand for approximated equilibrium shapes. They were measured only on the tube side and are, in general, different for the two sides of the segregated parts of the system.

Taking the mid-penetration force estimates (from Fig S7B) for the entire configurations space for both direct and indirect methods, we construct two concluding diagrams seen in Fig S8. The first diagram represents the total maximal mid-penetration force calculated at the bead surface as a function of the Young's modulus of the nuclear shell $E_s$. The second diagram represents the result of determination, based on the maximal mid-penetration force, of the number of actin filament end pushing a unit area of the bead. The area per actin filament end is $a_{filament} = A_{tot} / n_{filament}$ where $A_{tot} = \pi\left(1.75^2 - 1\right)\mu m^2$. The number of actin filament ends, $n_{filament}$, is derived by dividing the total force with the assumed force

that each actin filament generates as a result of polymerization ( $f_{filament} \sim 1pN$ ), $n_{filament} = f_z^{tot} / f_{filament}$ .

**Experimental Methods**

*Mice cells and their activation*

All experiments used C57/Bl6 mice or transgenic B6.Cg-Tg (Hist1H2BB/EGFP) mice. The H2B-EGFP transgenic mouse was purchased from The Jackson laboratory (http://jaxmice.jax.org). These mice express the H2B protein fused to EGFP under the chicken beta-actin promoter coupled to CMV immediate early promoter/enhancer. As a result all nucleated cells in the mouse have fluorescence. $CD4^+$ naïve T-cells were isolated from spleen of 8-10 week old mice using MagCellect isolation kit (R&D Systems, MN). $1X10^5$ cells were stimulated with antigen coated beads (Invitrogen, CA) at a stoichiometry of 1:2 (cell:bead).

*Immunostaining*

For staining, cells were activated on poly-d-lysine coated glass bottom dishes, fixed with 1% PFA for 20 minutes, permeabilized with 0.2% NP-40 for 5 minutes and blocked with 10mg/ml BSA for 1 hour at room temperature. Actin was stained using rhodamine phalloidin and DNA with Hoechst 33342 (Sigma).

*Confocal imaging*

Zeiss (LSM510-Meta) or Olympus FV1000 confocal fluorescence microscopes were used for imaging experiments using 63X/ 1.4 N.A oil immersion objective. 8-bit images of 512-by-512 pixels were acquired with 1 airy-unit pinhole aperture size and a z-step size of 500 nm. Time-lapse live cell images were recorded at 5 seconds/frame, with stage temperature maintained at $37^OC$ and $CO_2$ concentration maintained at 5%. 488nm laser line was used to excite EGFP or Alexa 488 tagged proteins, 543nm for rhodamine phalloidin and 405nm for Hoechst 33342.

**Supporting References**


1. Attard MM. 2003. Finite strain—isotropic hyperelasticity. International Journal of Solids and Structures 40(17):4353-4378.
2. Simo JC, Pister KS. 1984. Remarks on rate constitutive equations for finite deformation problems: computational implications. Computer Methods in Applied Mechanics and Engineering 46(2):201-215.
3. Holzapfel G. 2000. Nonlinear Solid Mechanics: A Continuum Approach for Engineering: John Wiley and Sons.
4. Truesdell C, and Noll, W. 2004. The Non-Linear Field Theories of Mechanics: Springer-Verlag Berlin Heidelberg New York


**Supplementary Movie S1.** Time-lapse imaging of H2B EGFP labeled T-cell activation by surrogate antigen-coated beads. Images were recorded at 5 seconds per frame.

Fig. S1

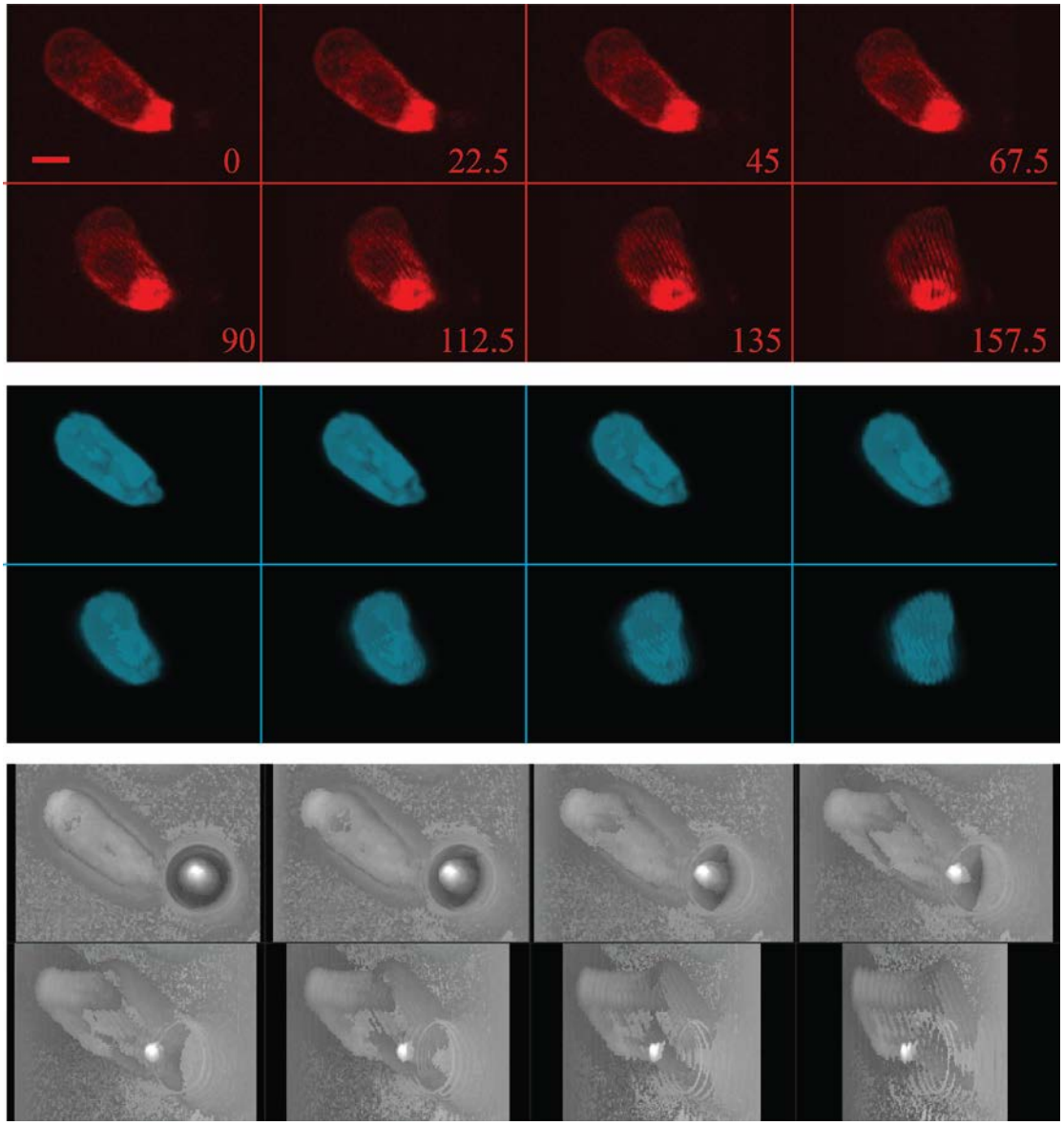


Fig. S1. 3D projection image of actin (red), DNA (blue) and bright-field (grey) for a representative cell with elongated cellular and nuclear architecture depicting the hollow actin tube. The numbers in red indicate the projection angle. Note the position of actin tube with respect to bead position seen in bright-field image. Scale bar 2μm.

Fig. S2

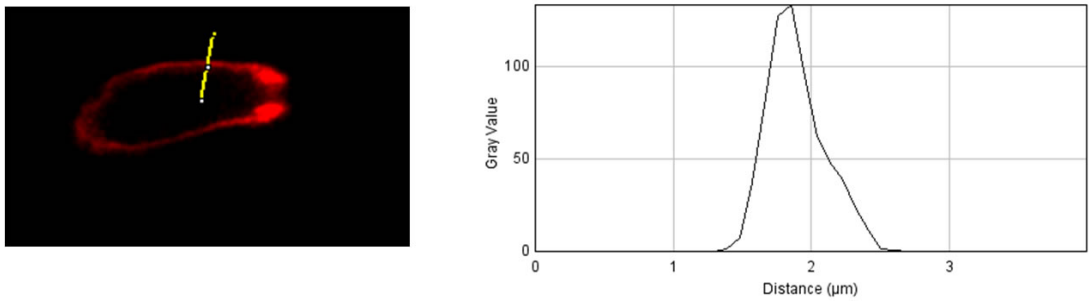


Fig S2. Actin stained image (red) of a T-cell with a line drawn across (yellow) (left panel). The corresponding intensity plot for this line is shown (right panel), from which the thickness of actin layer was determined.

Fig. S3

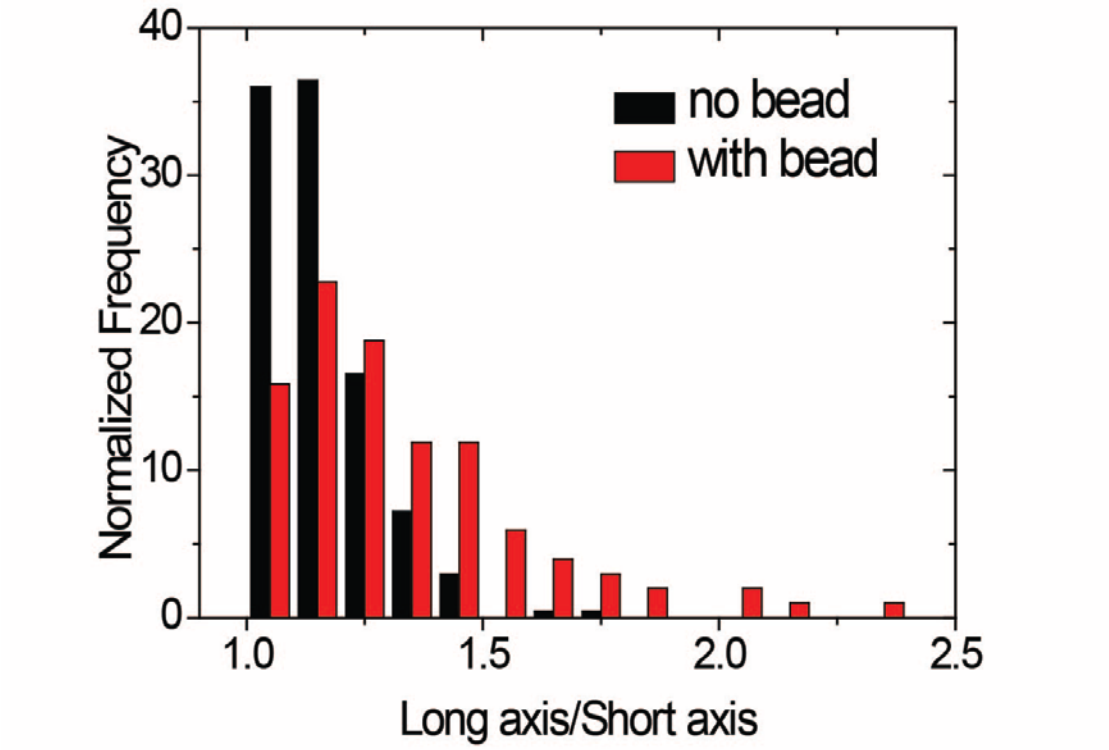


Fig S3. Graph showing the aspect ratio of nucleus for T-cells which do not make contact with bead (black) and those which make contact with beads (red). The maximum nuclear aspect ratio observed was ~2:1.

Fig. S4

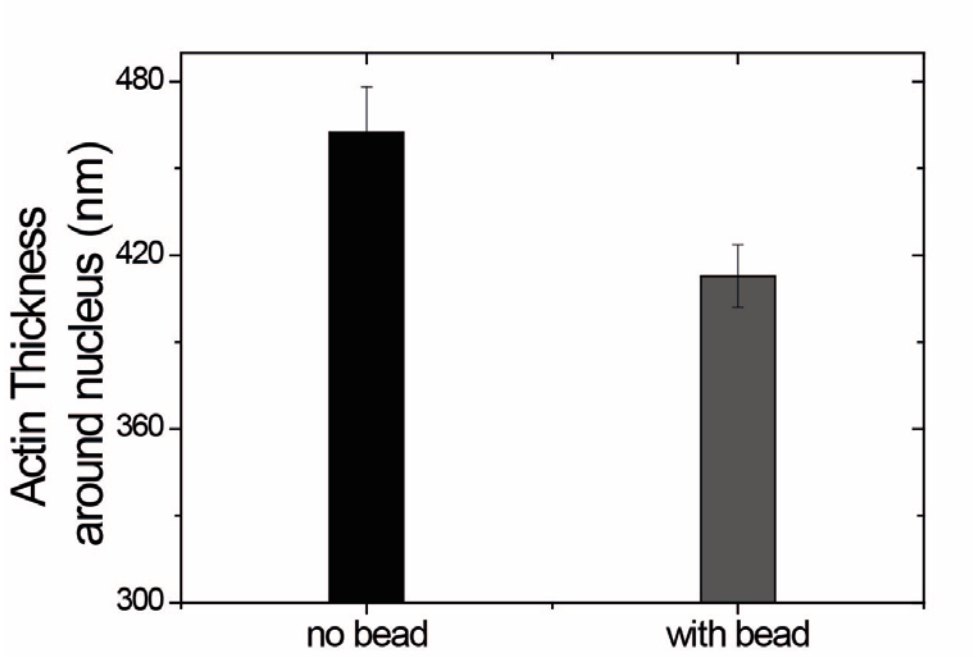


Fig. S4. Thickness of actin layer around the nucleus in cells without bead contact and those with bead contact and deformed nucleus. (n=50-60). SE plotted.

Fig. S5

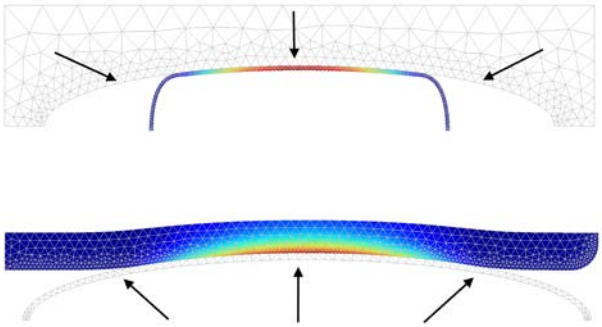

Fig. S5. Splitting the analysis into two complementary parts implemented in Finite Element Method. Lower panel - an infinitely rigid ellipsoid pushing from the inside on the actin tube. Upper panel - an infinitely rigid concave scaffold pressing on the nucleus shell. Both contours are mutually varied till a contact is found.

Fig. S6

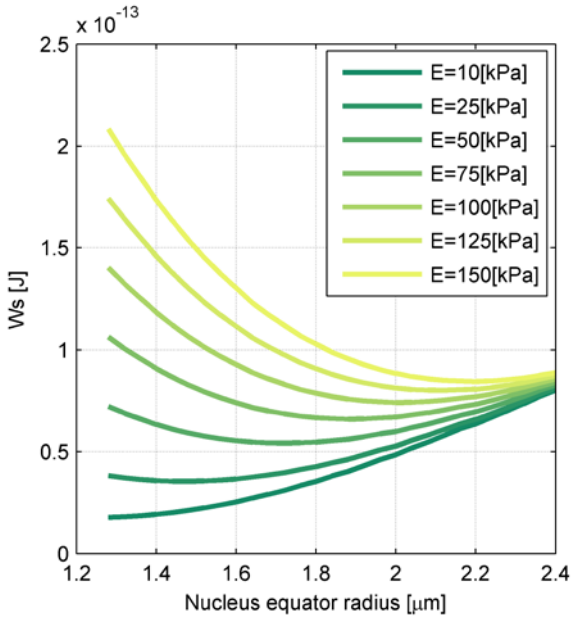


Fig. S6. The dependence of the total elastic strain energy on the final values of the equator radius of the nucleus. Different curves denote different values of the nucleus shell Young's modulus, $E_s$, for a given Poisson ratio $\nu_s = 0.1$.

Fig. S7

A

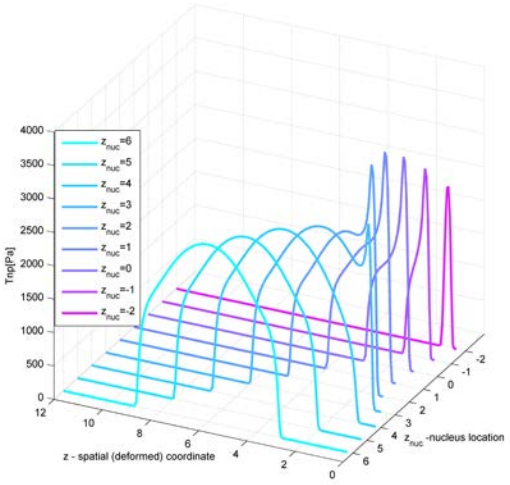


B

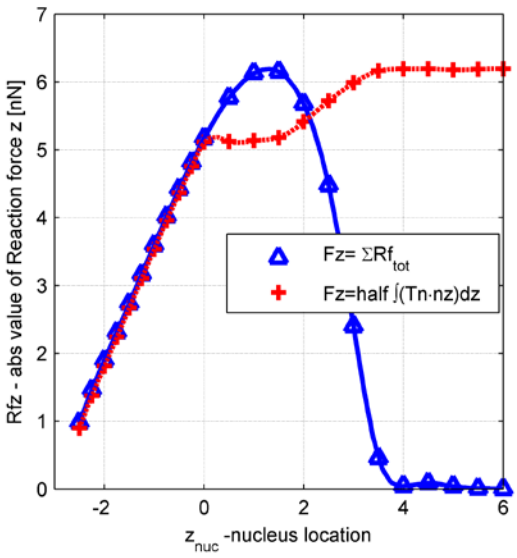


Fig. S7. Estimation of the axial reaction force at the bead surface using direct and indirect methods. (A). Contact pressure profiles measured on the deforming boundary as the nucleus moves away from the center of the actin tube towards the free edge. (B). Mid-penetration reaction force measured in two ways: (i) Directly at the bead surface (blue line) (ii) Indirectly by integration over half the contact pressure profile-projected on the $\hat{z}$ axis (red line). Both parts of the figure were calculated for an equator radius $a = 1.72\mu m$ with elastic moduli $E_s = 50kPa$ and $\nu_s = 0.1$.

Fig.S8

A

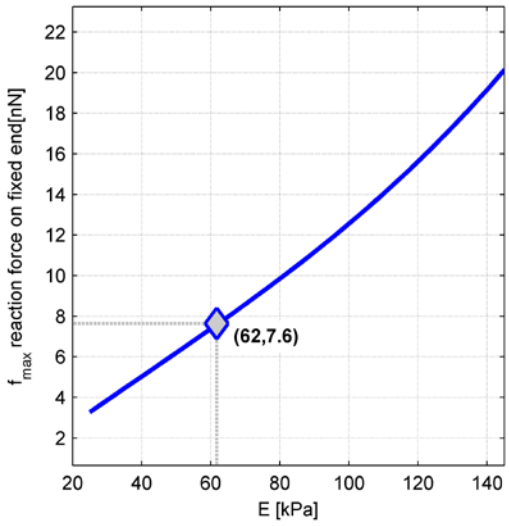


B

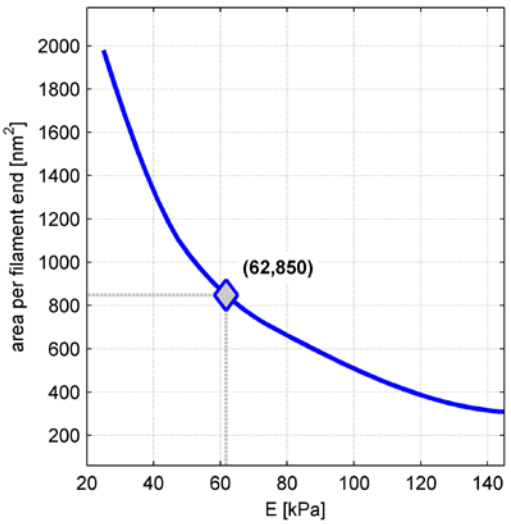


Fig. S8. Maximal force and actin filament spacing at the bead surface as function of the nucleus shell Young's modulus, $E_s$. The best fitted observed ratio of the deformed nucleus axes (2:1) corresponding to $E_s \sim 60kPa$ is marked on both diagrams. (A). Mid-penetration maximal (axial) reaction force measured in $nN$. (B). Lateral area per actin filament end at the bead surface in $nm^2$.